# An efficient kinetic modeling of electrons with nonlocal Ohm's law in plasmas relevant to inertial confinement fusion by using the AWBS transport equation

M. Holec,* V. Tikhonchuk, J.-L. Feugeas, and Ph. Nicolai
*Centre Lasers Intenses et Applications,*
*Universite de Bordeaux-CNRS-CEA,*
*UMR 5107, F-33405 Talence, France.*

P. Loiseau and A. Debayle
*CEA, DAM, DIF, F-91297 Arpajon Cedex, France.*

J. Brodrick and Ch. Ridgers
*Plasma Institute, York,*
*UK.*

B. Dubroca
*, Universite de Bordeaux,*
*France.*

R. Kingham
*Imperial College, Lodon,*
*UK.*

(Dated: October 2, 2018)

# Abstract

The interaction of lasers with plasmas very often leads to nonlocal transport conditions, where the classical hydrodynamic model fails to describe physical phenomena related to highly mobile particles. In this study the electron distribution in plasma is investigated for the conditions relevant to ICF. In particular, we focus on the transport of nonlocal (supra-thermal) electrons streaming down the temperature gradient in the ablating plasma. Nevertheless, the nature of plasma (ionized gas) requires a correct response of background electrons too. This is achieved by the action of an electric field, which provides a self-consistent Ohms law based on the kinetic modeling.Our approach leans on the Albritton-Williams-Bernstein-Swartz collision operator providing a simple, computationally efficient, transport equation of electrons and is further benchmarked against Vlasov-Fokker-Planck codes Aladin and Impact and collisional PIC code Calder.


## I. INTRODUCTION

The first attempts of modern kinetic modeling of plasma can be tracked back to the fifties, when Cohen, Spitzer, and Routly (CSR) [1] demonstrated that the effect of Coulomb collisions between electrons and ions in the ionized gas predominantly results from frequently occurring events of cumulative small deflections rather than occasional close encounters. This effect was originally described by Jeans in [2] and Chandrasekhar [3] proposed to use the diffusion equation model of the Vlasov-Fokker-Planck type (VFP) [4].

A classical paper by Spitzer and Harm (SH) [5] provides the computation of the electron distribution function (EDF) in a plasma (from low to high $Z$) with a temperature gradient accounting for e-e and e-i collisions. The expressions for current and heat flux are widely used in every plasma hydrodynamic models. The distribution function based on the spherical harmonics method in its first approximation (P1) [6] is of the form $f^0+\mu f^1$, where $f^0$ and $f^1$ are isotropic and $\mu$, is the direction cosine between the particle trajectory and some preferred direction in space. It should be emphasized that the SH solution expresses a small perturbation of equilibrium, i.e. that $f^0$ is the Maxwell-Boltzmann distribution and $\mu f^1$ represents a very small anisotropic deviation. This approximation holds for $L_T \gg \lambda_e$, a condition which is often invalid in laser plasmas, where $L_T$ is the temperature length scale and $\lambda_e$ the mean free path of electrons.

The actual cornerstone of the modern VFP simulations was set in place by Rosen-


* holec1@llnl.gov

bluth [7], when he derived a simplified form of the VFP equation for a finite expansion of the distribution function, where all the terms are computed according to plasma conditions, including $f^0$, which of course needs to tend to the Maxwell-Boltzmann distribution. Consequently, the pioneering work on numerical solution of the VFP equation [8, 9] revealed the importance of the nonlocal electron transport in laser-heated plasmas. In particular, ~~that~~ the heat flow down steep temperature gradients in unmagnetised plasma cannot be described by the classical, local fluid description of transport [5, 10]. ~~This is due to the classical $f^1$ is not a small deviation (especially for electrons faster than thermal velocity), i.e. $f^0 \sim f^1$, since the nonlocal regime is characterized by $L_T \sim \lambda_e$.~~ It was also shown that a thermal transport inhibition [8] ~~on one hand side,~~ and a nonlocal preheat ~~on the other hand side~~, naturally appear. These effects are attributed to significant deviations of $f^0$ from Maxwellian distribution.

Nevertheless, numerical solution of the VFP equation even in the Rosenbluth formalism remains very challenging computationally, because the e-e collision integral is nonlinear. More simple linear forms of e-e collision operator are needed.

It is the purpose of this paper to present an efficient alternative to VFP model based on the Albritton-Williams-Bernstein-Swartz collision operator (AWBS) [11]. In Section II we propose a modified form of the AWBS collision operator~~, where its~~ important properties are further presented in Section III with the emphasis on its comparison to the full VFP solution in local diffusive regime. Section V focuses on the performance of the AWBS transport equation model compared to modern kinetic codes including VFP codes Aladin and Impact [12], and PIC code Calder [13], where the cases related to real laser generated plasma conditions are studied. Finally, the most important outcomes of our research are concluded in Section VI.

## II. THE AWBS KINETIC MODEL

The electrons in plasma can be modeled by the deterministic Vlasov model of charged particles

$$\frac{\partial f}{\partial t} + \boldsymbol{v}\cdot\nabla_{\boldsymbol{x}} f + \frac{q_e}{m_e}\left(\boldsymbol{E} + \frac{\boldsymbol{v}}{c}\times\boldsymbol{B}\right)\cdot\nabla_{\boldsymbol{v}} f = C_{ee}(f) + C_{ei}(f), \tag{1}$$

where $f(t, \boldsymbol{x}, \boldsymbol{v})$ represents the density function of electrons at time $t$, spatial point $\boldsymbol{x}$, and velocity $\boldsymbol{v}$, $\boldsymbol{E}$ and $\boldsymbol{B}$ are the electric and magnetic fields in plasma, $q_e$ and $m_e$ being the charge and mass of electron.

The general form of the e-e collision operator $C_{ee}$ is the Fokker-Planck form published by Landau [14]

$$C_{FP}(f) = \Gamma \int \nabla_{\boldsymbol{v}} \nabla_{\boldsymbol{v}} (\boldsymbol{v} - \tilde{\boldsymbol{v}}) \cdot (f \, \nabla_{\tilde{\boldsymbol{v}}} f - f \, \nabla_{\boldsymbol{v}} f) \, \mathrm{d}\tilde{\boldsymbol{v}}, \tag{2}$$

where $\Gamma = \frac{4\pi q_e^4 \ln\Lambda}{m_e^2}$ and $\ln\Lambda$ is the Coulomb logarithm. The e-i collision operator $C_{ei}$ could be expressed in a simpler form since massive ions are considered to be motionless compared to electrons. The scattering operator accounts for the change of electron velocity without change in the velocity magnitude. It is expressed in spherical coordinates as

$$C_{ei}(f) = \frac{\nu_{ei}}{2} \left( \frac{\partial}{\partial \mu} \left( (1 - \mu^2) \frac{\partial f}{\partial \mu} \right) + \frac{1}{\sin^2 \phi} \frac{\partial^2 f}{\partial \theta^2} \right), \tag{3}$$

where $\mu = \cos\phi$, $\phi$ and $\theta$ are the polar and azimuthal angles, and $\nu_{ei} = \frac{Z n_e \Gamma}{v^3}$ is the e-i collision frequency.

The e-e collision operator needs to be linearized for efficient computations. Fish introduced a linear form of $C_{ee}$ in [15] in the high-velocity limit ($v \gg v_{th}$) electron collision operator

$$C_H(f) = v \nu_e \frac{\partial}{\partial v} \left( f + \frac{v_{th}^2}{v} \frac{\partial f}{\partial v} \right) + \frac{\nu_e}{2} \left( 1 - \frac{v_{th}^2}{2 v^2} \right) \left( \frac{\partial}{\partial \mu} \left( (1 - \mu^2) \frac{\partial f}{\partial \mu} \right) + \frac{1}{\sin^2 \phi} \frac{\partial^2 f}{\partial \theta^2} \right) \tag{4}$$

where $\nu_e = \frac{n_e \Gamma}{v^3}$ is the e-e collision frequency and $v_{th} = \sqrt{\frac{k_B T_e}{m_e}}$ is the electron thermal velocity. The linear form of $C_H$ arises from an assumption that the fast electrons predominantly interact with the thermal (slow) electrons, which simplifies importantly the form (2). However the diffusion term in the e-e collision operator (4) still presents numerical difficulties.

A yet simpler form of the collision operator of electrons was proposed in [16]

$$C_{AWBS}(f) = v \nu_e^* \frac{\partial}{\partial v} (f - f_M) + \frac{\nu_{ei} + \nu_e^*}{2} \left( \frac{\partial}{\partial \mu} \left( (1 - \mu^2) \frac{\partial f}{\partial \mu} \right) + \frac{1}{\sin^2 \phi} \frac{\partial^2 f}{\partial \theta^2} \right), \tag{5}$$

where $f_M = \frac{n_e}{(2\pi)^{\frac{3}{2}} v_{th}^3} \exp\left( -\frac{v^2}{2 v_{th}^2} \right)$ is the Maxwell-Boltzmann equilibrium distribution. Here, the first term representing the AWBS operator [11] accounts for relaxation to equilibrium due to the e-e collisions, and the second term accounts for the e-i and e-e collisions contribution to scattering.

A method of angular momenta for the solution of the electron kinetic equation with the collision operator (5) was introduced in [16, 17].

In (5) we have introduced a modified e-e collision frequency $\nu_e^*$ in order to address a proper behavior with respect to $Z$~~, which is~~ further analyzed in Section III and promising results compared to the full FP operator are presented.

## III. BGK, AWBS, AND FOKKER-PLANCK MODELS IN LOCAL DIFFUSIVE REGIME

An approximate solution to the so-called *local diffusive regime* of electron transport can be found~~, since the *diffusive regime* refers to a low anisotropy given by the projection $\mu$. i.e. modeled by a simple~~ P1 form ~~of EDF~~

$$\tilde{f}(z, v, \mu) = f^0(z, v) + \mu f^1(z, v), \quad (6)$$

where $z$ is the spatial coordinate along the axis $z$, $v$ the magnitude of transport velocity, and $\mu = \cos\phi$, where $\phi$ is the pitch angle with respect to the axis $z$.

The approximate transport solution is ~~then~~ obtained when analyzing ~~the action of~~ the time-steady ~~form~~ of (1) in 1D ~~on~~ the approximation (6) ~~as~~

$$\mu \left( \frac{\partial \tilde{f}}{\partial z} + \frac{q_e E_z}{m_e v} \frac{\partial \tilde{f}}{\partial v} \right) + \frac{q_e E_z}{m_e} \frac{(1-\mu^2)}{v^2} \frac{\partial \tilde{f}}{\partial \mu} = \frac{1}{v} C(\tilde{f}), \quad (7)$$

where $C$ is a given collision operator including both e-e and e-i collisions.

The locality of transport ~~is the best expressed~~ in terms of the Knudsen number $Kn = \frac{\lambda}{L}$, where $\lambda$ is the mean free path of electron and $L$ the characteristic length scale of plasma. ~~Consequently, p~~lasma conditions characterized by $Kn \ll 1$ exhibit a local transport regime. This measure then play a very important role in our analysis, where we use the electron~~i~~-electron and electron-ion mean free paths $\lambda_e = Z\lambda_{ei} = \frac{v}{\nu_e}$, and the density and temperature plasma scale lengths $L_{n_e} = n_e / \frac{\partial n_e}{\partial z}$ and $L_{T_e} = T_e / \frac{\partial T_e}{\partial z}$.

### A. The BGK local diffusive electron transport

Bhatnagar, Gross, and Krook introduced a ~~very simple form~~ of ~~a~~ collision operator [18]

$$C_{BGK}(\tilde{f}) = \nu_e(\tilde{f} - f_M) + \frac{\nu_{ei} + \nu_e}{2} \frac{\partial}{\partial \mu} (1-\mu^2) \frac{\partial \tilde{f}}{\partial \mu}. \quad (8)$$

In spite of its simple form, BGK collision operator (8) serves as a useful model providing a relevant kinetic response, yet only qualitative with respect to the FP collision operator (2). In particular, the conservation of kinetic energy, momentum, and number of particles is often violated [19].

However, the form of (8) provides a simple analytical treatment of local diffusive transport regime, when used in (7). As a result, ~~one finds a simple form of~~ the BGK isotropic and anisotropic terms of (6) ~~to be~~

$$f^0 = f_M + Kn \frac{v_{th}^2}{v^2} f^1, \quad (9)$$

$$f^1 = -\frac{\lambda_e}{Z} \left( \frac{\partial f^0}{\partial z} + \frac{q_e E_z}{m_e v} \frac{\partial f^0}{\partial v} \right), \quad (10)$$

where $Kn = \frac{\lambda_e}{L_{n_e}} + \frac{5}{2} \frac{\lambda_e}{L_{T_e}}$ ~~and a~~ detailed derivation of (9) and (10) can be found in Appendix A. Equation (9) states that $f^0 \rightarrow f_M$ when $Kn \ll 1$, and accordingly, $f^1 \rightarrow -\frac{\lambda_e}{Z} \left( \frac{\partial f_M}{\partial z} + \frac{q_e E_z}{m_e v} \frac{\partial f_M}{\partial v} \right)$. When the quasi-neutrality constraint on the electric field (A7) is used, ~~one finally obtains~~ the analytical BGK form of (6)

$$\tilde{f}_{BGK} = f_M - \mu \left( \frac{v^2}{2 v_{th}^2} - 4 \right) \frac{1}{Z} \frac{\lambda_e}{L_{T_e}} f_M, \quad (11)$$

which recovers the Lorentz electron-ion collision gas model [20]. It should be noticed that $f^0$ equilibrates to $f_M$ as $O(Kn^2)$ in (9), since $f^1 = \left( \frac{v^2}{2 v_{th}^2} - 4 \right) \frac{1}{Z} Kn f_M$.

The details about the BGK distribution function compared to other collision operators can be found in Section III D.

### B. The AWBS local diffusive electron transport

Similarly to the BGK model, the AWBS collision operator 5 explicitly uses equilibration to the Maxwell-Boltzmann distribution $f_M$. ~~On the other hand side~~ AWBS originates from $C_H$, which is derived from the full FP operator (2). ~~This makes the~~ AWBS operator ~~to be superior~~ ~~to~~ the BGK operator, which is considered a pure phenomenological model.

~~If (5) is used in (7), one obtains~~ the following ~~equations~~ governing the AWBS isotropic and anisotropic terms of (6)

$$\frac{\partial f^0}{\partial v} = \frac{\partial f_M}{\partial v} + Kn \frac{v_{th}^2}{v^2} \frac{f^1}{v}, \quad (12)$$

$$\frac{\partial f^1}{\partial v} - \frac{Z + \xi}{v \xi} f^1 = \frac{\lambda_e}{v \xi} \left( \frac{\partial f^0}{\partial z} + \frac{q_e E_z}{m_e v} \frac{\partial f^0}{\partial v} \right), \quad (13)$$

where $\xi$ represents a scaling parameter defining the modified e-e collision frequency as $\nu_e^* = \xi \nu_e$. A detailed derivation of (12) and (13) can be found in Appendix A. ~~One observes~~ that $f^0$ goes to ~~Maxwellian~~ when the local regime of transport is settled. Indeed, according to equation (12) the derivative $\frac{\partial f^0}{\partial v} \to \frac{\partial f_M}{\partial v}$ when $Kn \ll 1$ for any electron velocity, thus leading to $f^0 \to f_M$. Consequently, one finds the AWBS model equation for $f^1$ in local diffusive regime to be

$$\frac{\partial f^1}{\partial v} + \frac{Z + \xi}{v \xi} f^1 = \frac{\lambda_e}{v \xi} \left( \frac{1}{L_{n_e}} + \left( \frac{v^2}{2 v_{th}^2} - \frac{3}{2} \right) \frac{1}{L_{T_e}} - \frac{q_e E_z}{m_e v_{th}^2} \right) f_M. \quad (14)$$

Since there is no simple analytical ~~formula for $f^1$ solving~~ (14), we adopt the implicit Euler numerical integration with $\Delta v < 0$, i.e. we integrate from high electron velocity ($v_{max} = 7 v_{th}$) to the velocity equal to zero (using $10^4$ steps). This mimics a particle deceleration due to collisions. The correct numerical solution of (14) corresponds to an appropriate value of $E_z$ leading to a zero current. As in the BGK case, the numerical solution of (14) reveals that $f^1 \sim Kn f_M$ and that $f^0$ equilibrates to $f_M$ as $O(Kn^2)$ based on (12).

The details about the AWBS distribution function compared to other collision operators and a proper evaluation of the scaling parameter $\xi$ can be found in Section III D.

### C. The Fokker-Planck local diffusive electron transport

The solution to the 1D transport equation (7) using the Fokker-Planck collision operator (2) is very ambitious, as demonstrated in [1, 3, 7], fortunately, one can use the explicit evaluation of the electron distribution function published in [5], which takes the following form

$$f^1(z,v) = \frac{v_{2th}^4}{\Gamma Z n_e} \left(2\tilde{D}_T\left(\frac{v}{v_{2th}}\right) + \frac{3}{2}\frac{\gamma_T}{\gamma_E}\tilde{D}_E\left(\frac{v}{v_{2th}}\right)\right)\frac{f_M}{T}\frac{\partial T_e}{\partial z}, \tag{15}$$

where $\tilde{D}_T(x) = ZD_T(x)/B$, $\tilde{D}_E(x) = ZD_E(x)/A$, $\gamma_T$, and $\gamma_E$ are numerical values in TABLE I, TABLE II, and TABLE III in [5], and $v_{2th} = \sqrt{\frac{k_B T_e}{2m_e}}$.

One should be aware, that the solution of (7) ~~equipped~~ with the full FP collision operator reveals the importance of e-e Coulomb collisions, which is emphasized in the $Z$ dependence of the distribution function, current, heat flux, electric field, etc. In particular, the latter exhibits the following dependence [5]

$$\boldsymbol{E} = \frac{m_e v_{th}^2}{q_e}\left(\frac{\nabla n_e}{n_e} + \left(1 + \frac{3}{2}\frac{Z+0.477}{Z+2.15}\right)\frac{\nabla T_e}{T_e}\right), \tag{16}$$

which for $Z \gg 1$ corresponds to the classical Lorentz electric field (A7).

### D. Summary of the BGK, AWBS, and Fokker-Planck local diffusive transport

Ever since the SH paper [5], the effect of microscopic electron transport on the current $\int q_e \boldsymbol{v}\tilde{f}\,\mathrm{d}\boldsymbol{v}$ and the heat flux $\int \frac{m_e|\boldsymbol{v}|^2}{2}\boldsymbol{v}\tilde{f}\,\mathrm{d}\boldsymbol{v}$ in plasmas under local diffusive conditions has been understood. By overcoming some delicate aspects of the numerical solution to (2) presented in the CSR paper [1], the effect of electron-electron collisions was properly quantified and the correct dependence on $Z$ of the heat flux $\boldsymbol{q}$ was approximated as [5, 21]

$$\boldsymbol{q} = \frac{Z+0.24}{Z+4.2}\boldsymbol{q}_L, \tag{17}$$

where $\boldsymbol{q}_L = \kappa T_e^{\frac{5}{2}}\nabla T_e$ is the heat flux given by Lorentz gas model [20]. In the case of the BGK operator and its EDF formula (11), the correct dependence on $Z$ can be simply achieved by scaling the e-e and e-i collision frequencies as

$$\nu_e^{BGK} = \frac{\nu_{ei}^{BGK}}{Z} = \frac{Z+4.2}{Z+0.24}\nu_e, \tag{18}$$

which imposes a right heat flux magnitude (17).

We have performed an extensive computational analysis in the case of the AWBS operator in order to obtain the heat flux behavior while varying $Z$. As expected, the heat flux magnitude did not match exactly the $Z$-dependence (17), e.g. for $Z = 1$ the AWBS heat flux was about 60% less than the SH calculation, while there was a perfect match in

| | $Z=1$ | $Z=2$ | $Z=4$ | $Z=16$ | $Z=116$ |
|---|---|---|---|---|---|
| $\bar{\Delta}\boldsymbol{q}_{AWBS}$ | 0.057 | 0.004 | 0.037 | 0.021 | 0.004 |
| $\phi(Z)$ | -0.037 | -0.003 | 0.04 | 0.058 | 0.065 |

TABLE I. Relative error $\bar{\Delta}\boldsymbol{q}_{AWBS} = |\boldsymbol{q}_{AWBS} - \boldsymbol{q}_{SH}|/\boldsymbol{q}_{SH}$ of the $\nu_e^* = \frac{\nu_e}{2}$ scaling used in the AWBS model (5) showing the discrepancy (maximum around 6%) with respect to the original solution of the heat flux given by numerical solution in Spitzer and Harm [5]. The values of $\phi(Z)$ (weak dependence) are also shown.

the case of $Z \gg 1$. By assuming that the e-e collisions are responsible for this inadequacy, we searched for a scaling of $\nu_e$ in (5). Interestingly, we found an almost constant scaling $\xi$, i.e. with a very weak dependency on $Z$ as

$$\nu_e^* = \xi \nu_e = \left(\frac{1}{2} + \phi(Z)\right) \nu_e \approx \frac{\nu_e}{2}, \qquad (19)$$

where the dependence $\phi(Z) = \frac{0.59Z - 1.11}{8.37Z + 5.15} \ll \frac{1}{2}$ for any $Z$. Indeed, TABLE I shows $\phi(Z)$ and its corresponding relative error (maximum around 6%) of the heat flux modeled by (5) vs. SH results represented by (17). It should be noted that the error is calculated with respect to original values presented in TABLE III in [5]. It is worth mentioning, that the zero current condition was followed in all AWBS calculations. The overall result is that the consistent electric field is always almost equal to the classical Lorentz value (A7) with the difference being less than 0.01 % for any $Z$.

~~Nevertheless,~~ the electron-electron collisions effect represented by (17) provides only an integrated information about the heat flux magnitude. ~~If one takes a~~ clos~~ure~~ look at the distribution function itself~~,~~ the ~~conformity of~~ the modified AWBS collision operator ~~is even more emphasized as can be seen in~~ FIG. 1 ~~showing~~ the flux moment in spherical coordinates of velocity $q_1 = \frac{m_e v^2}{2} v f^1 v^2$. In the case of the high $Z$ Livermorium plasma ($Z = 116$), AWBS exactly aligns with the Lorentz gas limit. In the opposite case of the low $Z$ Hydrogen plasma ($Z = 1$), the AWBS distribution function approaches significantly the numerical SH solution. BGK takes the Lorentz gas distribution function form for any $Z$ only taking into account the scaling (18).

It is worth mentioning that the first derivative term in the AWBS collision operator (5) (red dashed line) provides a significant model improvement with respect to the SH (Fokker-Planck) solution (solid black line) compared to the simplest BGK model (8) (dashed-dot blue line) in FIG. 1.

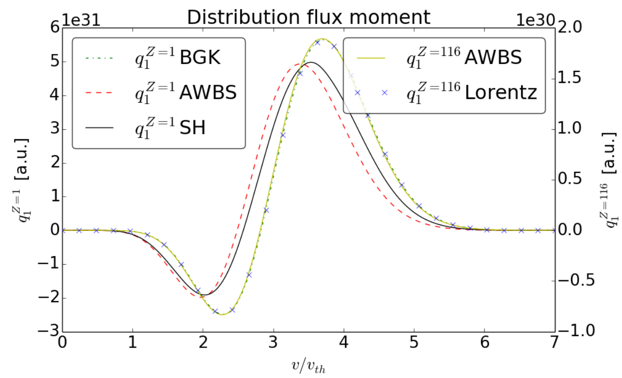


FIG. 1. The flux velocity moment of the anisotropic part of the electron distribution function in low $Z = 1$ and high $Z = 116$ plasmas in diffusive regime.

## IV. THE AWBS NONLOCAL TRANSPORT MODEL OF ELECTRONS

In order to define a nonlocal transport model of electrons, we use the AWBS collision operator and the P1 angular discretization of the electron distribution function

$$\tilde{f}(\boldsymbol{x}, \boldsymbol{n}, v) = f_0(\boldsymbol{x}, v) + \boldsymbol{n} \cdot \boldsymbol{f_1}(\boldsymbol{x}, v), \quad (20)$$

consisting of the isotropic part represented by the zeroth angular moment $f_0 = \frac{1}{4\pi}\int_{4\pi} \tilde{f} \mathrm{d}\boldsymbol{n}$ and the directional part represented by the first angular moment $\boldsymbol{f_1} = \frac{3}{4\pi}\int_{4\pi} \boldsymbol{n}\tilde{f} \mathrm{d}\boldsymbol{n}$, where $\boldsymbol{n}$ is the transport direction (the solid angle). Then, the first two angular moments [19] applied to the steady form of (1) with collision operator (5) (extended by (19)) lead to the model equations

$$v\frac{\nu_e}{2}\frac{\partial}{\partial v}\left(f_0 - f_M\right) = \frac{v}{3}\nabla \cdot \boldsymbol{f_1} + \frac{q_e}{m_e}\frac{\boldsymbol{E}}{3} \cdot \left(\frac{\partial \boldsymbol{f_1}}{\partial v} + \frac{2}{v}\boldsymbol{f_1}\right), \quad (21)$$

$$v\frac{\nu_e}{2}\frac{\partial \boldsymbol{f_1}}{\partial v} - \nu_{scat}\boldsymbol{f_1} = v\nabla f_0 + \frac{q_e}{m_e}\boldsymbol{E}\frac{\partial f_0}{\partial v} + \frac{q_e\boldsymbol{B}}{m_e c} \times \boldsymbol{f_1}, \quad (22)$$

where $\nu_{scat} = \nu_{ei} + \frac{\nu_e}{2}$. The system of equations (21) and (22) is called the **AP1 model** (AWBS + P1).

~~On the one hand side AP1 model gives us with the information about the electron distribution function, on the other hand side a macroscopic interpretation of the microscopic EDF properties are of great importance and provide the bridge between kinetic and fluid description of plasma~~. For example the *flux* quantities as electric current and heat flux due to the motion of electrons

$$\boldsymbol{j} = \frac{4\pi}{3}q_e \int v\boldsymbol{f_1}\,\mathrm{d}\tilde{v}, \quad \boldsymbol{q}_h = \frac{4\pi}{3}\frac{m_e}{2}\int v^3\boldsymbol{f_1}\,\mathrm{d}\tilde{v},$$

where $\mathrm{d}\tilde{v} = v^2\mathrm{d}v$ the spherical coordinates metric, are based on corresponding velocity moments (integrals) of the first angular moment of EDF. Consequently, the explicit formula for the first angular moment from (22) proves to be extremely useful

$$\boldsymbol{f_1} = \frac{\nu_{scat}^2\boldsymbol{F}^* + \boldsymbol{\omega}_B\ \boldsymbol{\omega}_B \cdot \boldsymbol{F}^* - \nu_{scat}\ \boldsymbol{\omega}_B \times \boldsymbol{F}^*}{\nu_{scat}(\boldsymbol{\omega}_B^2 + \nu_{scat}^2)}, \quad (23)$$

because it provides a valuable information about the dependence of macroscopic *flux* quantities on electric and magnetic fields in plasma, where $\boldsymbol{\omega}_B = \frac{q_e \boldsymbol{B}}{m_e c}$ is the electron gyrofrequency and $\boldsymbol{F}^* = v \frac{\nu_e}{2} \frac{\partial \boldsymbol{f_1}}{\partial v} - v \nabla f_0 - \frac{q_e}{m_e} \boldsymbol{E} \frac{\partial f_0}{\partial v}$.

### A. Nonlocal Ohm's law

~~The expression (23) becomes extremely useful when used to describe the electron fluid momentum, i.e. the current velocity moment~~

$$\boldsymbol{j}(f, \boldsymbol{E}, \boldsymbol{B}) = q_e \int v \boldsymbol{f_1} v^2 \, \mathrm{d}v = -\frac{q_e^2}{m_e} \int v \frac{\nu_{ei}^2 \boldsymbol{E}^* + \boldsymbol{\omega}_B \, \boldsymbol{\omega}_B \cdot \boldsymbol{E}^* + \nu_{ei} \, \boldsymbol{\omega}_B \times \boldsymbol{E}^*}{\nu_{ei}(\boldsymbol{\omega}_B^2 + \nu_{ei}^2)} \, \mathrm{d}\tilde{v}, \tag{24}$$

where $\boldsymbol{E}^* = \boldsymbol{E} \, \frac{\partial f_0}{\partial v} + \frac{m_e}{q_e} v \nabla f_0$ is the effective electric field in plasma. ~~We refer to (24) as to the **nonlocal Ohm's law**.~~ Its relation and a proper local asymptotic to the standard Ohm's law can be found when $f_0 \to f_M$ and no magnetic field ($\boldsymbol{\omega}_B = 0$) is considered. Then (24) simplifies to

$$\boldsymbol{j} = -\cancel{\frac{q_e^2}{m_e}} \int \cancel{\frac{v^3}{\nu_{ei}}} \left( \cancel{\boldsymbol{E} \, \frac{\partial f_M}{\partial v} + \frac{m_e}{q_e} v \nabla f_M} \right) \cancel{\mathrm{d}v =} \frac{16 \sqrt{\frac{2}{\pi}} q_e^2 k_B^{\frac{3}{2}} T_e^{\frac{3}{2}}}{m_e^{\frac{5}{2}} \Gamma Z} \left[ \boldsymbol{E} - \frac{\frac{5}{2} n_e k_B \nabla T_e + \nabla n_e k_B T_e}{q_e n_e} \right], \tag{25}$$

which can be directly compared to the fluid theory represented by the *generalized Ohm's law*

$$\boldsymbol{E} = \frac{\nabla p_e - \boldsymbol{R}_{T_e}}{q_e n_e} + \frac{\boldsymbol{j}}{\sigma}, \tag{26}$$

while addressing properly the pressure $p_e = n_e k_B T_e$, the thermal force $\boldsymbol{R}_{T_e} = -\frac{3}{2} n_e k_B \nabla T_e$ and the electrical conductivity $\sigma = \frac{16 \sqrt{\frac{2}{\pi}} q_e^2 k_B^{\frac{3}{2}} T_e^{\frac{3}{2}}}{m_e^{\frac{5}{2}} \Gamma Z}$ [10]. The local dependence of the AP1 current (25) on electric field and gradients of $n_e$ and $T_e$ clearly demonstrates, that (26) is a local version of (24).

A local version of the **nonlocal Ohm's law** (24) compared to the *generalized Ohm's law* (26) when a magnetic field is applied would require a much more delicate analysis and we leave it as a future complementary work.

It should be noted, that $\nu_e$-related terms in (23) have been omitted in (24), since the e-e collisions do not contribute (cancel out when integrated over velocity) to the momentum change, i.e. $\int v \left( v \frac{\nu_e}{2} \frac{\partial \boldsymbol{f_1}}{\partial v} - \frac{\nu_e}{2} \boldsymbol{f_1} \right) \mathrm{d}\tilde{v} = 0$.

### B. AWBS Nonlocal Transport Hydrodynamics

The *AWBS nonlocal transport hydrodynamic model* refers to two temperature single-fluid hydrodynamic model ~~extended by a~~ kinetic model of electrons using the AWBS transport equation~~, which provides a direct coupling between hydrodynamics~~ and Maxwell equations. Mass, momentum density, and total energy $\rho$, $\rho \boldsymbol{u}$, and $E = \frac{1}{2} \rho \boldsymbol{u} \cdot \boldsymbol{u} + \rho \varepsilon_i + \rho \varepsilon_e$, where $\rho$ is the ~~density of plasma,~~ $\boldsymbol{u}$ the plasma fluid velocity, $\varepsilon_i$ the specific internal ion energy density, and $\varepsilon_e$ the specific internal electron energy density, are modeled by the Euler equations in Lagrangian frame

$$\frac{\mathrm{d}\rho}{\mathrm{d}t} = -\rho\nabla\cdot\boldsymbol{u}, \tag{27}$$

$$\rho\,\frac{\mathrm{d}\boldsymbol{u}}{\mathrm{d}t} = -\nabla(p_i + p_e) + \boldsymbol{j}(f,\boldsymbol{E},\boldsymbol{B})\times\boldsymbol{B}, \tag{28}$$

$$\rho\, C_{V_i}\frac{\mathrm{d}T_i}{\mathrm{d}t} = \left(\rho^2 C_{T_i} - p_i\right)\nabla\cdot\boldsymbol{u} - G(T_i - T_e), \tag{29}$$

$$\rho\, C_{V_e}\frac{\mathrm{d}T_e}{\mathrm{d}t} = \left(\rho^2 C_{T_e} - p_e\right)\nabla\cdot\boldsymbol{u} + G(T_i - T_e) - \nabla\cdot\boldsymbol{q}_h(f,\boldsymbol{E},\boldsymbol{B}) + Q_{\mathrm{IB}}, \tag{30}$$

where $T_i$ is the ~~temperature of ions~~, $T_e$ the ~~temperature of electrons~~, $p_i$ the ion pressure, $p_e$ the electron pressure, $\boldsymbol{q}_h$ the heat flux, $Q_{\mathrm{IB}}$ the inverse-bremsstrahlung laser absorption, and $G = \rho C_{V_e}\nu_{ei}$ is the ion-electron energy exchange rate. The thermodynamic closure terms $p_e$, $p_i$, $C_{V_i} = \frac{\partial\varepsilon_i}{\partial T_i}$, $C_{T_i} = \frac{\partial\varepsilon_i}{\partial\rho}$, $C_{V_e} = \frac{\partial\varepsilon_e}{\partial T_e}$, $C_{T_e} = \frac{\partial\varepsilon_e}{\partial\rho}$ are obtained from an equation of state (EOS), e.g. the SESAME equation of state tables [22, 23].

The magnetic and electric fields are modeled by Maxwell equations

$$\frac{1}{c}\frac{\mathrm{d}\boldsymbol{B}}{\mathrm{d}t} = -\nabla\times\boldsymbol{E}, \tag{31}$$

$$\frac{1}{c}\frac{\mathrm{d}\boldsymbol{E}}{\mathrm{d}t} = \nabla\times\boldsymbol{B} - \frac{4\pi}{c}\boldsymbol{j}(f,\boldsymbol{E},\boldsymbol{B}), \tag{32}$$

where the initial state of $\boldsymbol{B}$ and $\boldsymbol{E}$ obeys the Gauss law.

We have explicitly written the current and heat flux as dependent on electron kinetics, represented by the electron distribution function $f$, and electric and magnetic fields. ~~In principal,~~ $\boldsymbol{j}(f,\boldsymbol{E},\boldsymbol{B})$ and $\boldsymbol{q}_h(f,\boldsymbol{E},\boldsymbol{B})$ can be referred to as the *kinetic closure* and ~~is~~ provided by the **AP1 model** (21) and (22), where $f_M$ is given on the spatial profile of $T_e$ governed by (30).

The strategy of solving (21) and (22) resides in integrating $\frac{\partial f_0}{\partial v}$ and $\frac{\partial \boldsymbol{f_1}}{\partial v}$ along the velocity magnitude. This is done by starting the integration from infinite velocity ($v = 7v_{th}^{max}$) to zero velocity. The value $v_{th}^{max}$ equals the electron thermal velocity corresponding to the maximum electron temperature in the current profile of plasma. It should be noted~~,~~ that the backward integration concept is crucial for the model, ~~since~~ it corresponds to the deceleration of electrons due to collisions [24].

The aforementioned full model defines all quantities in the fluid frame.

## V. BENCHMARKING THE AWBS NONLOCAL TRANSPORT MODEL

After having shown several encouraging properties of the AWBS transport equation defined by (5) under local diffusive conditions in Sec. III, this section provides a broader analysis of the electron transport ~~and focuses on analysis its behavior~~ under variety of ~~conditions in plasmas~~. In principle, this is characterized by allowing that electron mean free path can be arbitrarily long, which leads to so-called nonlocal electron transport extensively investigated in numerous publications [8, 16, 25–29]. Among a variety of tests suitable for benchmarking the nonlocal electron transport models published [16, 17, 21, 30–32], we focus on conditions relevant to inertial confinement fusion plasmas generated by lasers.

We introduce our implementation of the AWBS nonlocal transport model presented in Sec. IV called AP1, where its results are further benchmarked against simulation results provided by Calder, a collisional Particle-In-Cell code, and by Aladin and Impact VFP codes. Their description follows in the next section.

**Calder PIC code**

In the limit of classical physics, a fluid description of the particle phase-space, including small angle binary collisions, can be described with the Maxwell equations (31), (32) coupled with the ion and electron Vlasov equations with the Landau-Beliaev-Budker collisions integral (LBB) [14, 33]

$$\frac{\partial f_\alpha}{\partial t} + \mathbf{v}\cdot\nabla_{\mathbf{x}} f_\alpha + q_\alpha\left(\mathbf{E} + \mathbf{v}\times\mathbf{B}\right)\nabla_{\mathbf{p}} f_\alpha = C_{LBB}(f_\alpha, f_\alpha) + \sum_\beta C_{LBB}(f_\alpha, f_\beta). \quad (33)$$

The LBB collision integral takes the form

$$C_{LBB}(f_\alpha, f_\beta) = -\frac{\partial}{\partial \mathbf{p}}\cdot\frac{\Gamma_{\alpha\beta}}{2}\left[\int \mathbf{U}(\mathbf{p},\mathbf{p}')\cdot\left(f_\alpha \nabla_{\mathbf{p}'} f'_\beta - f'_\beta \nabla_{\mathbf{p}} f_\alpha\right)\right] d^3\mathbf{p}', \quad (34)$$

where its relativistic kernel reads $\mathbf{U}(\mathbf{p},\mathbf{p}') = \frac{r^2/\gamma\gamma'}{(r^2-1)^{3/2}}$ $[(r^2-1)\mathbf{I} - \mathbf{p}\otimes\mathbf{p} - \mathbf{p}'\otimes\mathbf{p}' + r(\mathbf{p}\otimes\mathbf{p}' + \mathbf{p}'\otimes\mathbf{p})]$ with $\gamma = \sqrt{1+\mathbf{p}^2}$, $\gamma' = \sqrt{1+\mathbf{p}'^2}$ and $r = \gamma\gamma' - \mathbf{p}\cdot\mathbf{p}'$. The momentum $\mathbf{p}_\alpha$ ($\mathbf{p}_\beta$) is normalized to $m_\alpha c$ (resp. $m_\beta c$). The collision operator (34) tends to (2) in the non-relativistic limit. The aforementioned model is solved in 3D by the PIC code CALDER. [13, 34]. Brief description of the Calder code FIG. 3.

**Impact and Aladin VFP codes**

The PIC code is extremely expensive as the collisions require the description of the velocity space in 3 dimensions. Yet, a reduction of dimensions can be done by developing the distribution function in a cartesian tensor series, equivalent to a serie along the spherical harmonics [35] as follows:

$$f(t,\mathbf{x},\boldsymbol{v}) = f_0(t,\mathbf{x},v) + \boldsymbol{n}\cdot\boldsymbol{f}_1(t,\mathbf{x},v) + \boldsymbol{n}\otimes\boldsymbol{n} : \mathbf{f}_2(t,\mathbf{x},v) + .... \quad (35)$$

A $\mathrm{P}_n$ model refers to neglecting orders higher than $\mathbf{f}_n$. The distribution function approximation $f(t,\mathbf{x},\boldsymbol{v}) \approx f_0(t,\mathbf{x},v) + \boldsymbol{n}\cdot\boldsymbol{f}_1(t,\mathbf{x},v)$ coupled with the Landau-Fokker-Planck collisional operator (2), leads to the $\mathrm{P}_1$-VFP model [12, 35]:

$$\frac{\partial f_0}{\partial t} + \frac{v}{3}\nabla\cdot f_1 + \frac{q_e}{3 m_e v^2}\frac{\partial}{\partial v}\left(v^2 \boldsymbol{E}\cdot\mathbf{f}_1\right) = C^0_{ee}(f_0), \quad (36)$$

$$\frac{\partial \mathbf{f}_1}{\partial t} + v\nabla f_0 + \frac{q_e\boldsymbol{E}}{m_e}\frac{\partial f_0}{\partial v} + \frac{q_e\boldsymbol{B}}{m_e}\times\mathbf{f}_1 = -\nu_{ei}\mathbf{f}_1 \quad (37)$$

where for simplicity only the isotropic contribution of (2) is used

$$C_{ee}^0(f_0) = \frac{\Gamma}{v^2}\frac{\partial}{\partial v}\left[C(f_0)f_0 + D(f_0)\frac{\partial f_0}{\partial v}\right], \quad (38)$$

$$C(f_0(v)) = 4\pi\int_0^v f_0(u)u^2 \mathrm{d}u, \quad (39)$$

$$D(f_0(v)) = \frac{4\pi}{v}\int_0^v u^2\int_u^\infty w f_0(w)\mathrm{d}w\mathrm{d}u. \quad (40)$$

Impact and Aladin solve the system (36) and (37) with the Maxwell equations (31) and (32) in two dimensions, assuming motionless ions. Brief description of the Aladin code FIG. 4, FIG. 2.

### A. Heat-bath problem

The accuracy of the AP1 implementation is compared to Aladin, Impact and Calder codes by calculating the heat flow in the case where a large relative temperature variation

$$T_e(z) = 0.575 - 0.425\tanh\left((z-450)s\right), \quad (41)$$

which exhibits a smooth steep gradient at point 450 $\mu$m connecting a hot bath ($T_e$ = 1 keV) and cold bath ($T_e$ = 0.17 keV) and $s$ is the parameter of steepness. This test is referred to as a simple non-linear heat-bath problem and originally was introduced in [30] and further investigated in [16, 17, 31, 32].

The total computational box size is 700 $\mu$m in the case of Aladin and Impact and 1000 $\mu$m in the case of Calder. We performed Aladin, Impact, and Calder simulations showing an evolution of temperature

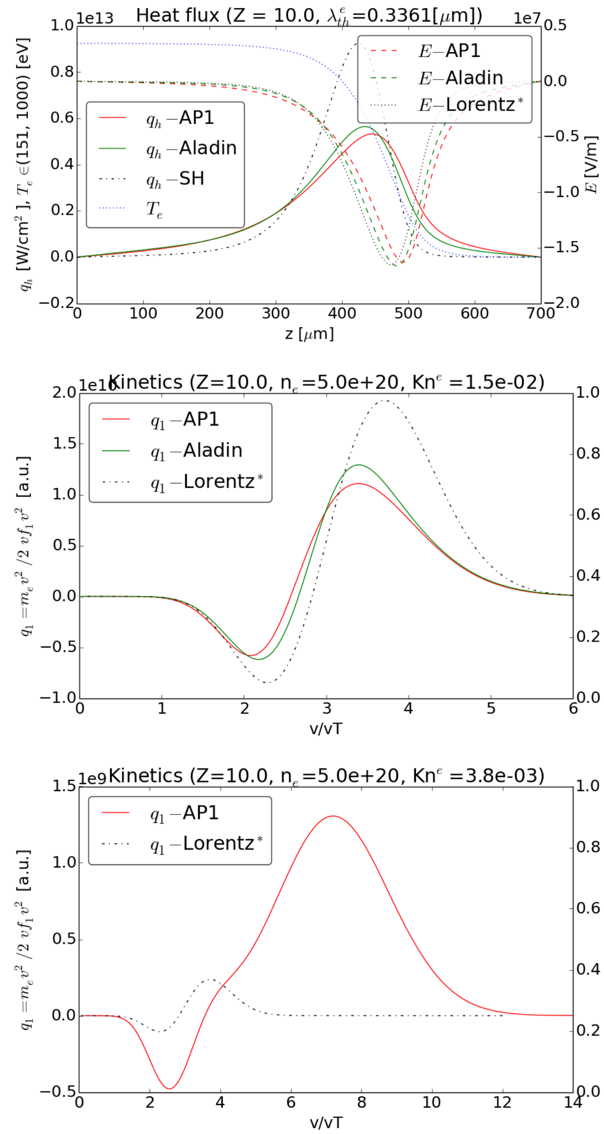


FIG. 2. Snapshot 12 ps. Top: correct steady solution of heat flux. Middle: correct comparison to kinetic profiles at point 442 $\mu$m by Aladin. Velocity limit 3.4 $v_{th}$. Bottom: correct comparison to kinetic profiles at point 550 $\mu$m by Aladin. Velocity limit 8.8 $v_{th}$

starting from the initial profile (41). Due to an inexact initial distribution function (approximated by Maxwellian), the first phase

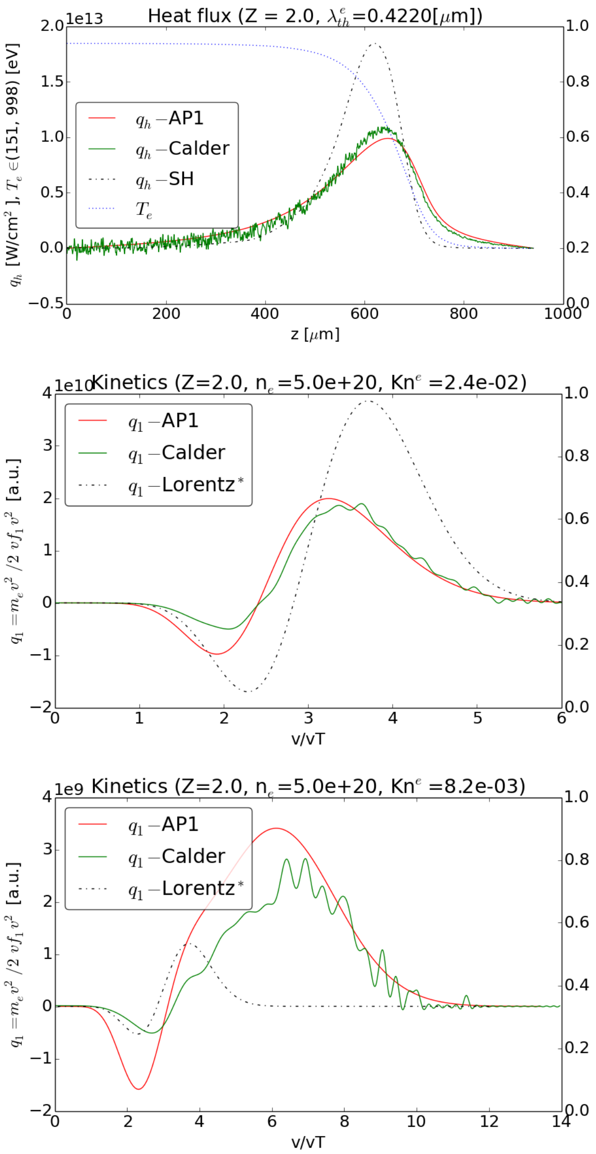


FIG. 3. Snapshot 11 ps. Left: correct steady solution of heat flux. Velocity limit 6.4 $v_{th}$.

of the simulation exhibits a transient behavior of the heat flux. After several ps the distribution adjusts properly to its nonlocal nature and the actual heat flux profile can be compared. We then take the temperature profile from Aladin/Impact/Calder and used our AP1 implementation to calculate the heat flow it would predict given this profile. In particular, the AP1 results corresponding to the evolved temperature profile by Aladin can be found in FIG. 4 and FIG. 2 for $Z = 1$ and $Z = 10$ respectively. The AP1 results computed on the evolved temperature profile for $Z = 2$ by Calder can be found in FIG. 3.

For all heat-bath simulations the electron density, Coulomb logarithm and ionisation were kept constant and uniform. The coulomb logarithm was held fixed throughout, $\ln\Lambda = 7.09$. Nevertheless, the Knudsen number $\mathrm{Kn}^e$ has been varied among the simulation runs in order to address a broad range of nonlocality of the electron transport corresponding to the laser-heated plasma conditions, i.e. $\mathrm{Kn}^e \in (0.0001, 1)$. The variation of $\mathrm{Kn}^e$ arises from the variation of the uniform electron density $n_e \in (10^{19}, 10^{23})$ cm$^{-3}$ or the length scale given by the slope of the temperature profile $s \in (1/2500, 1/25)\mu$m. Results of an extensive set of simulations of varying $\mathrm{Kn}^e$ is shown in FIG. 5.

Apart from the distribution function details related to the point of the heat flux maximum, in FIG. 4 we also present the detail of the kinetic profile at point 580 $\mu$m corresponding to a highly nonlocal nature of the heat flux profile. Here a good agreement with [31] can be found.

| $\mathrm{Kn}^e$ | $10^{-4}$ | $10^{-3}$ | $10^{-2}$ | $10^{-1}$ | 1 |
|---|---|---|---|---|---|
| $v_{lim}/v_{th}$ | 70.8 | 22.4 | 7.3 | 3.1 | 1.8 |

TABLE II. Scan over varying nonlocality ($\mathrm{Kn}^e$) showing the limit of the collision friction dominance over the acceleration of electrons due to the electric field force. The electric field effect is dominant for electrons with higher velocity than $v_{lim}$ defined in (B3). $\mathrm{Kn}^e$ and $v_{th}$ are evaluated from the same plasma profiles.

When analyzing the results of FIG. 5 we have found an interesting observation related to stopping effect of electrons. It turns out, that the force acting on electrons is dominated by electric field above some velocity limit $v_{lim}$ and this limit drops down significantly when the plasma conditions are more nonlocal, i.e. with increasing Knudsen number as can be seen in TABLE II.

For practical reasons we present in TABLE II some explicit values of velocity limit corresponding to varying transport conditions expressed in terms of "$Z$" Knudsen number $\mathrm{Kn}^e = \frac{\lambda_e}{\sqrt{Z+1} L_{T_e}}$, where $\sqrt{Z+1}$ provides a proper scaling of nonlocality with respect to ionization, i.e. the effect of scattering of electrons on ions [27].

In every simulation run of AP1 we used 250 velocity groups in order to avoid numerical errors in modeling of the electron kinetics. However, a smaller number of groups, e.g. 50, provides a very similar results (an error around 10% in the heat flux).

## B. Hohlraum problem

Additionally to the steep temperature gradients, the laser-heated plasma experiments also involve steep density gradients and variation in ionization, which is even more dominant in multi-material targets as in inertial fusion experiments, e.g. at the interface between the helium gas-fill and the ablated high $Z$ plasma.

In [32], a kinetic simulation of such a test was introduced. Plasma profiles provided by a HYDRA simulation in 1D spherical geometry of a laser-heated gadolinium hohlraum containing a typical helium gas-fill were used as input for the IMPACT [12] VFP code. Electron temperature $T_e$, electron density $n_e$ and ionisation $Z$ profiles shown in FIG. 6 at 20 nanoseconds of the HYDRA simulation were used (after spline smoothing) as the initial conditions for the IMPACT run (in planar geometry). For simplicity, the Coulomb logarithm was treated as a constant $\ln\Lambda_{ei} = \ln\Lambda_{ee} = 2.1484$. In reality, in the low-density corona lnΛ reaches 8, which, however, does not affect the heat flux profile significantly.

It is worth mentioning that in the surroundings of the heat flux maximum ($\sim$ 1662$\mu$m) the profiles of all plasma variables exhibit steep gradients with a change from $T_e$ = 2.5 keV, $n_e$ = 5×10$^{20}$ cm$^3$, $Z$ = 2 to $T_e$ = 0.3 keV, $n_e$ = 6×10$^{21}$ cm$^3$ , $Z$ = 44 across approximately 100 $\mu$m (between 1600 $\mu$m and 1700 $\mu$m), starting at the helium-gadolinium interface.

## VI. CONCLUSIONS

- The most important point is that we introduce a collision operator, which is coherent with the full FP, i.e. no extra dependence on $Z$.

- Touch pros/contras of linearized FP in Aladin and Impact vs AWBS

- Raise discussion about what is the weakest point of AP1 for high Kns: the velocity limit or phenomenological Maxwellization?

- Summarize useful outcomes related to plasma physics as the tendency of the velocity maximum in $q_1$ with respect to $Z$ and Kn$^e$.

- Emphasize the good results of Aladin (compared to Impact) and also outstanding results of Calder while being PIC.

## ACKNOWLEDGMENTS

## Appendix A: Background of the local diffusive regime theory

The left hand side of (7) acts on (6) as

$$\mu\left(\frac{\partial \tilde{f}}{\partial z} + \frac{q_e E_z}{m_e v}\frac{\partial \tilde{f}}{\partial v}\right) + \frac{q_e E_z}{m_e}\frac{1-\mu^2}{v^2}\frac{\partial \tilde{f}}{\partial \mu} = \mu\left(\frac{\partial f^0}{\partial z} + \frac{q_e E_z}{m_e v}\frac{\partial f^0}{\partial v}\right) + \frac{q_e E_z}{m_e v^2} f^1 + O(\mu^2). \tag{A1}$$

The action on (6) of the BGK operator (8) as used in (7) reads

$$\frac{1}{v}C_{BGK}(\tilde{f}) = \frac{\tilde{f} - f_M}{\lambda_e} + \frac{1}{2}\left(\frac{Z}{\lambda_e} + \frac{1}{\lambda_e}\right)\frac{\partial}{\partial \mu}(1-\mu^2)\frac{\partial \tilde{f}}{\partial \mu}, = \frac{f^0 - f_M}{\lambda_e} - \mu\frac{Z}{\lambda_e} f^1. \tag{A2}$$

Consequently, if the isotropic and anisotropic parts of (A1) and (A2) are compared, one finds the following equations

$$f^0 = f_M + \frac{\lambda_e q_e E_z}{m_e v^2} f^1, \tag{A3}$$

$$f^1 = -\frac{\lambda_e}{Z}\left(\frac{\partial f^0}{\partial z} + \frac{q_e E_z}{m_e v}\frac{\partial f^0}{\partial v}\right). \tag{A4}$$

It is valid to assume that $f^0 = f_M$ from (A3). Then,

$$f^1_{BGK} = -\frac{\lambda_e}{Z}\left(\frac{\partial f_M}{\partial z} + \frac{q_e E_z}{m_e v}\frac{\partial f_M}{\partial v}\right). \tag{A5}$$

The *quasi-neutrality* constraint, corresponding to a zero electric reads

$$\boldsymbol{j} \equiv q_e \int \boldsymbol{v} \tilde{f}\, \mathrm{d}\boldsymbol{v} = \boldsymbol{0}. \tag{A6}$$

In the case of the BGK EDF, in particular its anisotropic part (A5), the zero current condition takes the form

$$2\pi \int_{-1}^{1} \int_{v} v\mu^2 f^1_{BGK} \,\mathrm{d}v\mathrm{d}\mu = 0,$$

which leads to the electric field (same as the classical Lorentz electric field [20])

$$E_z = \frac{m_e v_{th}^2}{q_e} \left( \frac{1}{L_{n_e}} + \frac{5}{2}\frac{1}{L_{T_e}} \right). \tag{A7}$$

It is worth mentioning, that the deviation of $f^0$ from $f_M$ in (A3) can be written as $\left(\frac{\lambda_e}{L_{n_e}} + \frac{5}{2}\frac{\lambda_e}{L_{T_e}}\right)\frac{v_{th}^2}{v^2} f^1$, where naturally arises the Knudsen number $Kn = \frac{\lambda_e}{L_{n_e}} + \frac{5}{2}\frac{\lambda_e}{L_{T_e}}$ comprising both contributions of electron density and temperature gradients.

In the case of the AWBS operator (5) used in (7), its action on (6) reads

$$\begin{aligned}
\frac{1}{v} C_{AWBS}(\tilde{f}) &= \frac{v}{\lambda_e}\frac{\partial}{\partial v}\left(\tilde{f} - f_M\right) \\
&\quad + \frac{1}{2}\left(\frac{Z}{\lambda_e} + \frac{1}{\lambda_e}\right)\frac{\partial}{\partial \mu}(1-\mu^2)\frac{\partial \tilde{f}}{\partial \mu} \\
&= \frac{v}{\lambda_e}\frac{\partial}{\partial v}\left(f^0 - f_M\right) \\
&\quad + \mu\left(\frac{v}{\lambda_e}\frac{\partial f^1}{\partial v} - \frac{Z+1}{\lambda_e} f^1\right).
\end{aligned} \tag{A8}$$

One finds the following equations if the isotropic and anisotropic parts of (A1) and (A8) are compared

$$\frac{\partial}{\partial v}\left(f^0 - f_M\right) = \frac{\lambda_e q_e E_z}{m_e v^2}\frac{f^1}{v}, \tag{A9}$$

$$\frac{v}{\lambda_e}\frac{\partial f^1}{\partial v} - \frac{Z+1}{\lambda_e} f^1 = \frac{\partial f^0}{\partial z} + \frac{q_e E_z}{m_e v}\frac{\partial f^0}{\partial v} \tag{A10}$$

If we assume that $\frac{\partial f^0}{\partial v} = \frac{\partial f_M}{\partial v}$, i.e. $f^0 = f_M$, the anisotropic part of the AWBS operator is governed by the equation

$$\frac{\partial f^1_{AWBS}}{\partial v} - \frac{Z+1}{v} f^1_{AWBS} = \frac{\lambda_e}{v}\left(\frac{\partial f_M}{\partial z} + \frac{q_e E_z}{m_e v}\frac{\partial f_M}{\partial v}\right). \tag{A11}$$

Even though it is not straightforward, the electric field in (A11) (solved numerically) providing a zero current exactly matches (A7). Consequently, the deviation of $\frac{\partial f^0}{\partial v}$ from $\frac{\partial f_M}{\partial v}$ in (A9) can be written as $Kn\frac{v_{th}^2}{v^2}\frac{f^1}{v}$.

Finally, it should be stressed, that the concept of locality expressed as $Kn \ll 1$ is crucial for our *local diffusive regime* analysis, because it provides sufficient Maxwellization, i.e. (A3) and (A9), and correspondingly, (A5) and (A11) are valid models.

### Appendix B: AP1 electric field limit

Interestingly, we have encountered a very specific property of the AP1 model with respect to the electric field magnitude. The easiest way how to demonstrate this is to write the model equations (21) and (22) in 1D (z-axis). Then, due to its linear nature, it is easy to eliminate one of the partial derivatives with respect to $v$, i.e. $\frac{\partial f_0}{\partial v}$ or $\frac{\partial f_{1_z}}{\partial v}$. In the case of elimination of $\frac{\partial f_0}{\partial v}$ one obtains the following equation

$$\left(v\frac{\nu_e}{2}-\frac{2q_e^2E_z^2}{3m_e^2v\nu_e}\right)\frac{\partial f_{1_z}}{\partial v}=\frac{2q_eE_z}{3m_e\nu_e}\frac{\partial f_{1_z}}{\partial z}+\frac{4\pi q_eE_z}{3m_e}\frac{\partial f_M}{\partial v}$$
$$+\frac{v}{3}\frac{\partial f_0}{\partial z}+\left(\frac{4q_e^2E_z^2}{3m_e^2v^2\nu_e}+\left(\nu_{ei}+\frac{\nu_e}{2}\right)\right)f_{1_z}. \tag{B1}$$

It is convenient to write the bracket on the left hand side of (B1) as $\frac{2}{3v\nu_e}\left(\left(\sqrt{3}v\frac{\nu_e}{2}\right)^2-\frac{q_e^2}{m_e^2}E_z^2\right)$ from where it is clear that the bracket is negative if $\sqrt{3}v\frac{\nu_e}{2} < \frac{q_e}{m_e}|\boldsymbol{E}|$, i.e. there is a velocity limit for a given magnitude $|\boldsymbol{E}|$, when the collisions are no more fully dominant and the electric field introduces a comparable effect to the collision friction in the electron transport.

It can be shown, that the last term on the right hand side of (B1) is dominant and the solution behaves as

$$\Delta\boldsymbol{f_1}\sim\exp\left(\frac{\frac{4q_e^2E_z^2}{3m_e^2v^2\nu_e}+\left(\nu_{ei}+\frac{\nu_e}{2}\right)}{v\frac{\nu_e}{2}-\frac{2q_e^2E_z^2}{3m_e^2v\nu_e}}\Delta v\right), \tag{B2}$$

where $\Delta v<0$ represents a velocity step of the implicit Euler numerical integration of decelerating electrons. However, (B2) exhibits an exponential growth for velocities above the friction limit (bracket on the left hand side of (B1))

$$v_{lim}=\sqrt{\frac{\sqrt{3}\Gamma m_e}{2q_e}\frac{n_e}{|\boldsymbol{E}|}}, \tag{B3}$$

which makes the problem to be ill-posed.

In order to provide a stable model, we introduce a reduced electric field to be acting as the accelerating force of electrons

$$|\boldsymbol{E}_{red}|=\sqrt{3}v\frac{m_e}{q_e}\frac{\nu_e}{2}, \tag{B4}$$

ensuring that the bracket on the left hand side of (B1) remains positive. Further more we define two quantities

$$\omega_{red}=\frac{|\boldsymbol{E}_{red}|}{|\boldsymbol{E}|},\quad \nu_{scat}^E=\frac{q_e}{m_ev}\left(|\boldsymbol{E}|-|\boldsymbol{E}_{red}|\right),$$

introducing the reduction factor of the electric field $\omega_{red}$ and the compensation of the electric field effect in terms of scattering $\nu_{scat}^E$. Consequently, the AP1 model (21), (22), and (**??**) can be formulated as well posed with the help of $\omega_{red}$ and $\nu_{scat}^E$. Nevertheless, before doing so, we introduce a slightly different approximation to the electron distribution function as

$$\tilde{f}=\frac{4\pi f_M+\delta f_0}{4\pi}+\frac{3}{4\pi}\boldsymbol{n}\cdot\boldsymbol{f_1}. \tag{B5}$$

where $\delta f_0$ represents the departure of isotropic part from the Maxwell-Boltzmann equilibrium distribution $f_M$. Then, the stable AP1 model reads

$$v\frac{\nu_e}{2}\frac{\partial\delta f_0}{\partial v}=v\nabla\cdot\boldsymbol{f_1}+\frac{q_e}{m_e}\boldsymbol{E}\cdot\left(\omega_{red}\frac{\partial\boldsymbol{f_1}}{\partial v}+\frac{2}{v}\boldsymbol{f_1}\right) \tag{B6}$$

$$v\frac{\nu_e}{2}\frac{\partial\boldsymbol{f_1}}{\partial v}=\tilde{\nu}_{scat}\boldsymbol{f_1}+\frac{v}{3}\nabla\left(4\pi f_M+\delta f_0\right)$$
$$+\frac{q_e\boldsymbol{E}}{3m_e}\left(4\pi\frac{\partial f_M}{\partial v}+\omega_{red}\frac{\partial\delta f_0}{\partial v}\right), \tag{B7}$$

where $\tilde{\nu}_{scat}=\nu_{ei}+\nu_{scat}^E+\frac{\nu_e}{2}$.

The reason for keeping $f_M$ in the distribution function approximation (B5) can be seen in the last term on the right hand side of (B7), which provides the effect of electric field on directional quantities as current or heat flux. In principle, the explicit use of $f_M$ ensures the proper effect of $\boldsymbol{E}$ if $\delta f_0 \ll f_M$, i.e. no matter what the reduction $\omega_{red}$ is. Apart from its stability, it also exhibits much better convergence of the electric field, which is now given by the zero current condition of (B7) as

$$\boldsymbol{E} = \frac{\int_v \left( \frac{\nu_e}{2\tilde{\nu}_{scat}} v^2 \frac{\partial \boldsymbol{f_1}}{\partial v} - \frac{v^2}{3\tilde{\nu}_{scat}} \nabla \left( 4\pi f_M + \delta f_0 \right) \right) v^2 \, \mathrm{d}v}{\frac{q_e}{m_e} \int_v \frac{v}{3\tilde{\nu}_{scat}} \left( 4\pi \frac{\partial f_M}{\partial v} + \omega_{red} \frac{\partial \delta f_0}{\partial v} \right) v^2 \, \mathrm{d}v}. \tag{B8}$$


[1] R. S. Cohen, L. Spitzer, Jr., P. M. Routly, The electrical conductivity of an ionized gas, Phys. Rev. 80 (1950) 230–238.

[2] J. H. Jeans, Astronomy and Cosmogony, Cambridge University Press, London, 1929.

[3] S. Chandrasekhar, Stochastic problems in physics and astronomy, Rev. Mod. Phys. 15 (1943) 1.

[4] M. Planck, Über einen Satz der statistischen Dynamik und seine Erweiterung in der Quantentheorie, Sitzungsber. Preuss. Akad. Wiss. 24 (1917) 324–341.

[5] L. Spitzer, Jr. and R. Härm, Transport phenomena in a completely ionized gas, Phys. Rev. 89 (1953) 977.

[6] J. H. Jeans, The equations of radiative transfer of energy, Month. Not. Royal Astr. Soc. 78 (1917) 28–36.

[7] M. N. Rosenbluth, W. M. MacDonald, D. L. Judd, Fokker-planck equation for an inverse-square force, Phys. Rev. 107 (1957) 1.

[8] A. R. Bell, R. G. Evans, D. J. Nicholas, Phys. Rev. Lett. 46 (1981) 243.

[9] J. P. Matte, J. Virmont, Electron heat transport down steep temperature gradients, Phys. Rev. Lett. 49 (1982) 1936–1939.

[10] S. I. Braginskii, Transport processes in a plasma, Reviews of Plasma Physics 1 (1965) 205.

[11] J. R. Albritton, E. A. Williams, I. B. Bernstein, K. P. Swartz, Nonlocal electron heat transport by not quite maxwell-boltzmann distributions, Phys. Rev. Lett. 57 (1986) 1887–1890.

[12] R. J. Kingham, A. R. Bell, An implicit Vlasov-Fokker-Planck code to model nonlocal electron transport in 2-D with magnetic fields, J. Comput. Phys. 194 (194) (2004) 1–34.

[13] F. Perez, L. Gremillet, A. Decoster, M. Drouin, E. Lefebvre, Improved modeling of relativistic collisions and collisional ionization in particle-in-cell codes, Phys. Plas-

mas 19 (2012) 083104.

[14] L. Landau, Kinetic equation for the coulomb effect, Phys. Z. Sowjetunion 10 (1936) 154.

[15] N. J. Fish, Theory of current drive in plasmas, Rev. Mod. Phys. 59 (1987) 175.

[16] D. D. Sorbo, J.-L. Feugeas, P. Nicolai, M. Olazabal-Loume, B. Dubroca, S. Guisset, M. Touati, V. Tikhonchuk, Reduced entropic model for studies of multidimensional nonlocal transport in high-energy-density plasmas, Phys. Plasmas 22 (2015) 082706.

[17] D. D. Sorbo, J.-L. Feugeas, P. Nicolai, M. Olazabal-Loume, B. Dubroca, V. Tikhonchuk, Extension of a reduced entropic model of electron transport to magnetized nonlocal regimes of high-energy-density plasmas, Laser Part. Beams 34 (2016) 412–425.

[18] P. Bhatnagar, E. Gross, M. Krook, A Model for Collision Processes in Gases. I. Small Amplitude Processes in Charged and Neutral One-Component Systems, Phys. Rev. 94 (1954) 511–525.

[19] I. P. Shkarofsky, T. W. Johnston, M. P. Bachynskii, The particle Kinetics of Plasmas, Addison-Wesley, Reading, 1966.

[20] H. A. Lorentz, The motion of electrons in metallic bodies, in: Proceedings of the Royal Netherlands Academy of Arts and Sciences, Amsterdam, Vol. 7, 1905, pp. 438–453.

[21] E. M. Epperlein, R. W. Short, A practical nonlocal model for electron heat transport in laser plasmas, Phys. Fluids B 3 (1991) 3092–3098.

[22] T. Group, SESAME report on the Los Alamos equation-of-state library, Tech. Rep. Tech. Rep. LALP-83-4, Los Alamos National Laboratory, Los Alamos (1983).

[23] S. P. Lyon, J. D. Johnson, SESAME: The Los Alamos national laboratory equation of state database, Tech. Rep. LA-UR-92-3407, Los Alamos National Laboratory, Los Alamos (1992).

[24] M. Touati, J.-L. Feugeas, P. Nicolai, J. Santos, L. Gremillet, V. Tikhonchuk, A reduced model for relativistic electron beam transport in solids and dense plasmas, New J. Phys. 16 (2014) 073014.

[25] R. C. Malone, R. L. McCroy, R. L. Morse, Phys. Rev. Lett. 34 (1975) 721.

[26] D. G. Colombant, W. M. Manheimer, M. Busquet, Test of models for electron transport in laser produced plasmas, Phys. Plasmas 12 (2005) 072702.

[27] J. F. Luciani, P. Mora, J. Virmont, Nonlocal heat transport due to steep temeperature gradients, Phys. Rev. Lett. 51 (1983) 1664–1667.

[28] A. V. Brantov, V. Y. Bychenkov, V. T. Tikhonchuk, Nonlocal electron transport

in laser heated plasmas, Phys. Plasmas 5 (1998) 2742–2753.

[29] G. Schurtz, P. Nicolai, M. Busquet, A non-local electron conduction model for multidimensional radiation hydrodynamics codes, Phys. Plasmas 4238 (2000) 7.

[30] A. Marocchino and M. Tzoufras and S. Atzeni and A. Schiavi and Ph. Nicolai and J. Mallet and V. Tikhonchuk and J.-L. Feugeas, Comparison for non-local hydrodynamic thermal conduction models, Phys. Plasmas 20 (2013) 022702.

[31] M. Sherlock, J. P. Brodrick, C. P. Ridgers, A comparison of non-local electron transport models for laser-plasmas relevant to inertial confienement fusion, Phys. Plasmas 24 (2017) 082706.

[32] J. P. Brodrick, R. J. Kingham, M. M. Marinak, M. V. Patel, A. V. Chankin, J. T. Omotani, M. V. Umansky, D. D. Sorbo, B. Dudson, J. T. Parker, G. D. Kerbel, M. Sherlock, C. P. Ridgers, Testing nonlocal models of electron thermal conduction for magnetic and inertial confinement fusion applications, Phys. Plasmas 24 (2017) 092309.

[33] S. T. Beliaev, G. I. Budker, The Relativistic Kinetic Equation, Soviet Physics Doklady 1 (1956) 218.

[34] E. Lefebvre, et al, Nucl. Fusion 43 (2003) 629.

[35] T. W. Johnston, Cartesian tensor scalar product and spherical harmonic expansions in boltzmann's equation, Phys. Rev. 120 (1960) 1103–1111.

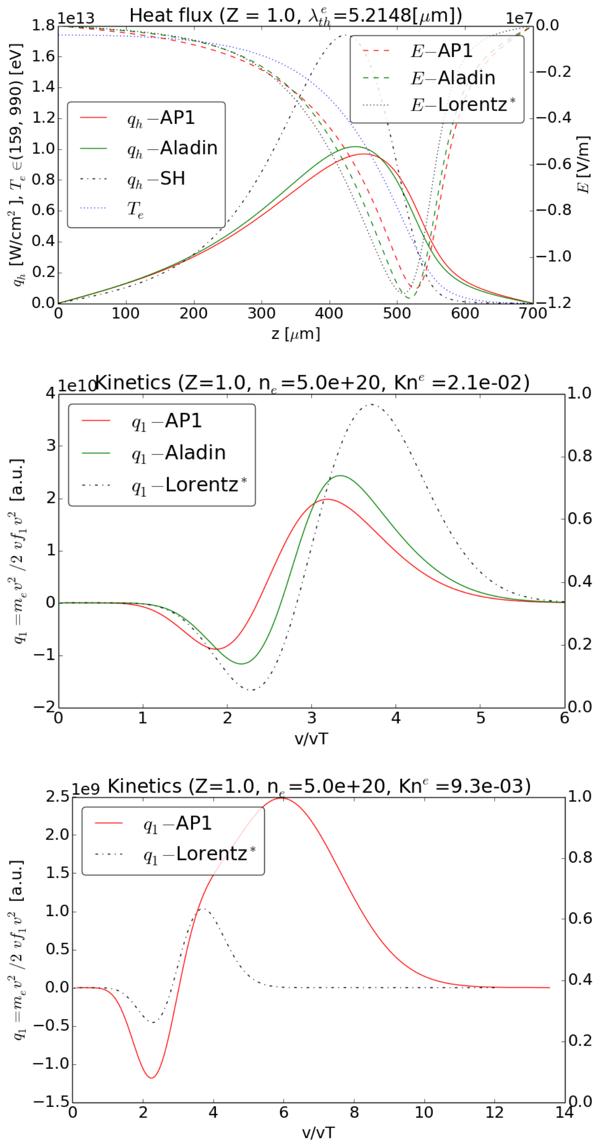


FIG. 4. Snapshot 20 ps. Top: correct steady solution of heat flux. Right: Aladins results are correct. Velocity limit 4.4 $v_{th}$. Snapshot 20 ps. AP1 kinetic profiles at point 580 $\mu$m corresponding to a highly nonlocal nature of the heat flux and is in a good agreement with [31]. Velocity $max(q_1) = 6.0\ v_{th}$. Velocity limit 9.0 $v_{th}$.

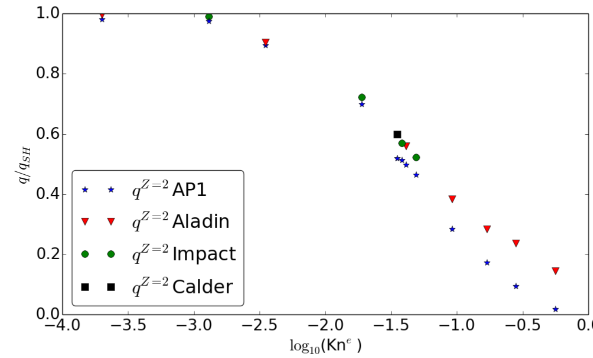


FIG. 5. Simulation results for the case $Z = 2$ computed by AP1/Aladin/Impact/Calder. Every point corresponds to the maximum heat flux in a "tanh" temperature simulation, which can be characterized by Kn. The range of $\log_{10}(\mathrm{Kn}) \in (0, -4)$ can be expressed as equivalent to the electron density approximate range $n_e \in (1e19, 3.5e22)$ of the 50 $\mu$m slope tanh case. In the case of $\mathrm{Kn} = 0.56$, $q_{Aladin}/q_{AP1} \approx 7.9$.

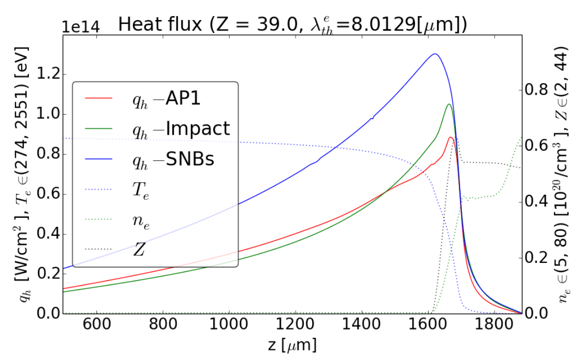


FIG. 6.